2018 26th Mediterranean Conference on Control and Automation (MED)
Zadar, Croatia, June 19-22, 2018

Relative Pose Estimation of Unmanned Aerial Systems

Athanasios Tsoukalas[1], Anthony Tzes[1] and Farshad Khorrami[2]

Abstract— **The relative accurate pose estimation problem of collaborating Unmanned Aerial Systems (UASs) in GPS-denied environments is addressed in this article. The on-board system uses fiducial markers attached in the facets of a truncated rhombicuboctahedron placed on top of the UAS. A visual marker-tracking mechanism using a global shutter camera is used to estimate the relative pose between the UASs under the Line-of-Sight (LoS) constraint. The pose estimator operates in parallel with an Ultra-wideband (UWB) system that transmits extremely short RF-pulses, spreading the radio energy over a wide frequency band, and measures the relative distance using Time Of Arrival (TOA) measurements from a set of off-board anchors. Experimental studies show that the UWB-system can provide satisfactory measurements at large distances (2m to 50m) but the resolution is not sufficient for operating the UASs in very short relative distances (under 5m). Therefore, the visual system is used to improve the relative position measurements at short distances (0.2m to 5m) in addition to providing orientation measurements.**

Keywords: Pose Determination, Localization, Unmanned Aerial Systems, Visual tracking, Fiducial Markers, RF-tracking, Ultra wide band tracking.

I. Introduction

Collaborative multi-agent systems ([1, 2]) typically require the relative pose between the team's members. Additionally, the relative precise position and orientation with reduced latency in its inference is of paramount importance in UAS-tasks [3].

Pose estimation techniques can be categorized as Exogenous and Endogenous. Exogenous methods include Receive Signal Strength Indicator (RSSI) ([4]), UWB-RF based (e.g., Pozyx) ([5–11]), Radar, LIDAR and visual methods ([12–16]). Endogenous methods include on board systems like Inertial Measurement Units (IMU), GPS and Differential GNSS ([17]).

In this work, a novel rhombicuboctahedron fiducial marker (Figure 1) based visual approach is used to determine the relative pose of moving drones. This solid contains squares and isosceles triangles as its facets, thus deeming it appropriate for identification of its attached fiducial markers. The utilization of this solid allows the concurrent observation of many fiducial markers resulting in a smaller pose estimation error. Each individual marker's attributes can be identified using the Aruco marker detection library ([18, 19]). Individual markers have been shown to work in a leader-follower UAS control scheme ([20]).

[1]The authors are with Electrical & Computer Engineering, New York University Abu Dhabi, Abu Dhabi 129188, United Arab Emirates athanasios.tsoukalas (anthony.tzes) @nyu.edu
[2]The author is with Electrical & Computer Engineering Department, New York University, Brooklyn, NY 11201, USA

In this work, we will focus on the visual aspect of the system, proposing a truncated rhombicuboctahedron arrangement to hold the fiducial markers, as shown in Figure 2. The concurrent computation of all markers' attributes (squares within facets) requires the use of an external add on to the Aruco library. The rhombicuboctahedron solid (75 gr weight) is attached on a UAS as well as a solid cube of the same facet areas to compare the pose determination results. We have shown that a more accurate pose determination can be achieved utilizing rhombicuboctahedron than a cube.

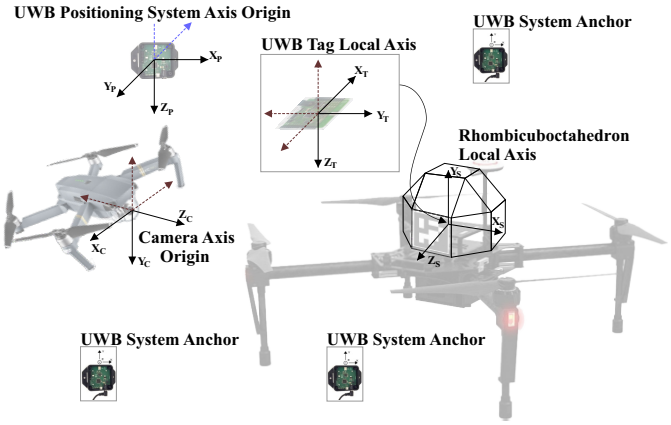

Fig. 1: UAS equipped with UWB-tag and fiducial markers.

To determine the relative position of moving drones, we are deploying an Ultra-Wide Band (UWB) positioning system (20gr weight). This UWB system has a range of about 50 meters with an accuracy of about 10cm. To improve the relative position measurement when the UASs are close to each other (i.e, within 5 meters), we augment the position measurements with the visual camera system using the fiducial markers. The position measurements from the two systems are fused. It should be noted that the UAS's orientation is strictly derived by the visual system. Figure 1 shows the arrangement of the attached rhombicuboctahedron and the UWB system anchor nodes and tags on the UASs.

Figure 2 shows members of the UAS-fleet (DJI Matrice and DJI Mavic Pro) with the attached rhombicuboctahedron with fiducial markers printed on its sides, which is used in combination with the Aruco-library to identify the approaching UAS pose in relation to a coordinate system attached to the UAS's camera. Experimental results showing pose accuracy that we have achieved are given in Section III. The position and orientation accuracy depends on the relative distance of UAVs as well as the size of rhumbicuboctahedorns utilized (this is limited by the size of the deployed UAS).

Fig. 2: Heterogeneous UASs with attached rhombicuboctahedron and fiducial markers.

II. Relative Pose Estimation Problem

The problem of identifying approaching UAS's relative pose with accuracy is a rather difficult one when these UASs are in near distance, due to the nature of the surrounding environment and the varying conditions ([21, 22]).

Classical methods like RSSI and GPS-based systems do not work satisfactorily, each having its own limitations. As an example, in the GPS case, there is need for the approaching UAS to broadcast its GPS-coordinates that are subject to a significant error (1m in GPS & 0.5m in GPS-RTK) resulting in significant latency. Furthermore, the on-board IMU-based localization systems can typically estimate the UAS orientation within a 3° (5° absolute roll/pitch/yaw) error that can be accumulated with the one from the observing UAS.

In this article, we propose a scheme where the relative position and orientation of UASs can be identified using visual feedback from the cameras attached on each UAS. This is also enhanced by using an UWB-position scheme, where each UAS knows and broadcasts its absolute position with respect to a ground coordinate system using RF-anchors.

As long as the observed UAS is within the camera's Field of View (FoV), it is searched for any fiducial markers. Under the assumption of the a priori knowledge of the markers' alphabet and their size, the relative pose can be estimated. Rather than relying on a single observed marker, the proposed rhombicuboctahedron offers 17 possible arrangements of markers placed in 13 square facets and 4 in the remaining equilateral triangular facets. In this way, the camera can observe a maximum of 9 facets (8 are occluded being in the unobserved sides of the solid), thus reducing the pose-estimation error. In most experimental cases, rather than observing 9 markers, the camera observed up to 6 markers on the rhumbicuboctahedorn (compared to a maximum of 3 for a cubic-solid). Since our fiducial marker alphabet offers 102 distinct members, then 6 (=102/17) distinct UASs can be observed using this scheme (without any additional features) by attaching different markers at each UAS.

To acquire knowledge of the UASs' positions in relation to a ground station, an Ultra Wide Band based positioning system is employed. The UWB method is used combined with the visual based method to improve the position estimation. Orientation is estimated by the camera system.

A. Visual pose estimation using fiducial markers

The fiducial marker identification scheme ([18, 19]) utilizes a special arrangement of squares inside a rectangle in order to identify and distinguish markers. The procedure of extracting the marker rectangle and identifying the marker code is composed of a number of steps.

The steps include a filtering process with local adaptive thresholding, for edge extraction, a contour extraction step followed by a polygonal approximation to distringuish the rectangular markers, a size based elimiination, marker code extraction and perseptive correction and thresholding followed by the marker identification and error correction to determine whether the identified marker belongs to a dictionary.

Each marker can be uniquely identified by the system, and both estimations of its position and orientation in relation to the camera are provided. Having identified the relative pose of each marker, the relative pose of the truncated rhombicuboctahedron is computed. Since this solid is attached to the UAS, the corresponding relative pose can be identified. The truncated rhombicuboctahedron, shown in Figure 3, with its 13 squares and 4 triangle facets has an area

$$\mathscr{A}_r = 13(a \times a) + 4\left(\frac{1}{2}a \times \left(a\sqrt{\frac{5}{4}}\right)\right)$$

where a is the square facet's edge length. The multiple markers allow for robustness in occlusion and lighting conditions

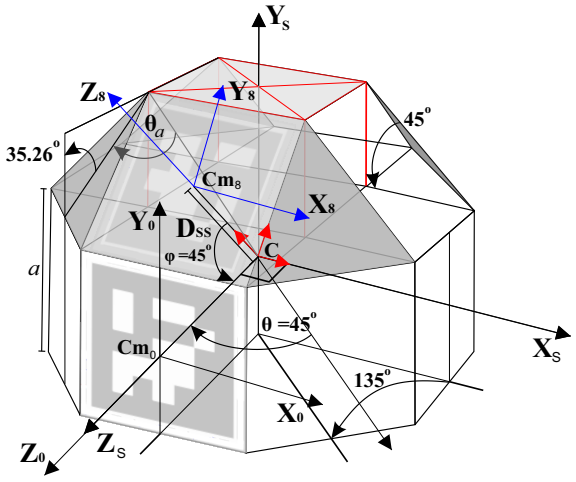

Fig. 3: Truncated rhombicuboctahedron geometry.

as the system can identify the pose given only a subset of the markers.

The homogeneous transformations that take place during the identification of the solid center that corresponds to each estimated marker position are in the following order: a) Translation from camera axes to the marker axes center C_{mi} using the Aruco provided translation matrix T_i^m, b) Rotation of the moved camera axes to align to the marker orientation using the Aruco provided rotation matrix R_i^m, and c) Combined translation and rotation from the identified square (triangular) facet corresponding to the identified marker to the center of the solid, using the matrix T_{mc}^s (T_{mc}^t) as follows

$$T_{mc}^s = \begin{bmatrix} c\theta_i & 0 & -s\theta_i & 0 \\ -s\phi_i \times s\theta_i & c\phi_i & -c\theta_i \times s\phi_i & 0 \\ c\phi_i \times s\theta_i & s\phi_i & c\phi_i \times c\theta_i & -a\frac{1+\sqrt{2}}{2} \\ 0 & 0 & 0 & 1 \end{bmatrix},$$

$$T_{mc}^t = \begin{bmatrix} c\theta_i & 0 & -s\theta_i & 0 \\ -s\phi_i \times s\theta_i & c\phi_i & -c\theta_i \times s\phi_i & p_y a \\ c\phi_i \times s\theta_i & s\phi_i & c\phi_i \times c\theta_i & p_z a \\ 0 & 0 & 0 & 1 \end{bmatrix}$$

where $s\theta$ ($c\theta$) corresponds to the $\sin(\theta)$ ($\cos(\theta)$), and

$$\begin{aligned} \theta_a &= 90^\circ - \arcsin(\sqrt{\frac{2}{3}}) + \arcsin\left(\frac{\sqrt{2}}{\sqrt{5+2\sqrt{2}}}\right) \\ p_y &= \frac{1}{2}\left(\sqrt{3} - \sqrt{5+2\sqrt{2}}\cos(\theta_a) - \frac{\sin(60^\circ)}{1+\sin(60^\circ)}\right) \\ p_z &= -\frac{\sqrt{5+2\sqrt{2}}}{2}\sin(\theta_a). \end{aligned}$$

The planar-rollover of the 17 facets with their associated markers are presented in Figure 4. Marker 0 corresponds to the one that has axis $Z_c = Z_0$ passing through its center as shown in Figure 3, and the angles θ_i and ϕ_i for each marker correspond to the horizontal and vertical axes, respectively.

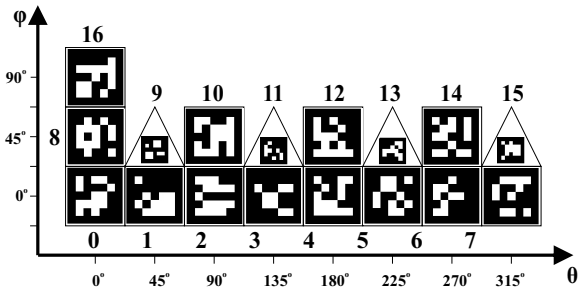

Fig. 4: Fiducial marker arrangement.

For the ith identified marker $i \in I_n \subset \{0,1,\ldots,16\}$, the estimated pose of the solid's center is computed as

$$T_i^s = \begin{bmatrix} T_i^m \times R_i^m \times T_{Mc}^s, \text{ for square facet} \\ T_i^m \times R_i^m \times T_{Mc}^t, \text{ for triangular facet.} \end{bmatrix}$$

Having identified (cardinality$(I_n) \leq 9$) the estimated solid's centers from all markers, a procedure is followed to identify and eliminate outliers based on the estimated angles and center-distances followed by a weighted average of the remaining ones.

B. UWB-based position estimation

The Ultra Wide Band based method is used for the RF based positioning. Specifically, the UWB devices are used for measuring distances between a tag UWB device attached on a UAS and N-base anchor UWB devices and estimate the tag's position using multilateration. Multiple tags may be used with a single anchor setup. The multilateration technique for computing the position from a number of range measurements for the 2D-case is presented in the following section.

Let p be the UWB tag 2D-position $p = [x,y]^T$ and assume the coordinates of each anchor position $p_i = [x_i, y_i]^T$, $i = 1,\ldots,N$. The distance between the ith anchor and the UWB Tag device is

$$d_i = \sqrt{(x-x_i)^2 + (y-y_i)^2},\ i = 1,\ldots,N. \quad (1)$$

The aforementioned set of equations can be cast in a matrix format as $b = A\begin{bmatrix} x \\ y \end{bmatrix}$, where

$$b = \begin{bmatrix} d_1^2 - x_1^2 - y_1^2 - d_N^2 + x_N^2 + y_N^2 \\ \vdots \\ d_{N-1}^2 - x_{N-1}^2 - y_{N-1}^2 - d_N^2 + x_N^2 + y_N^2 \end{bmatrix} \quad (2)$$

$$A = -2\begin{bmatrix} x_1 - x_N & y_1 - y_N \\ \vdots & \vdots \\ x_{N-1} - x_N & y_{N-1} - y_N \end{bmatrix}. \quad (3)$$

In the case where $N > 3$ anchors are available, the solution to the positioning problem can be inferred as

$$p = (A^T A)^{-1} A^T b\ . \quad (4)$$

III. Experimental studies

In the following section, we present the experimental findings when comparing the rhombicuboctahedron with an arrangement of markers placed at the five facets of a cube in various positions and orientations, along with measurements with the UWB system in the various vertical and horizontal angles versus the camera's axes.

A. Hardware specifications

The camera used for the experiments is an Odroid oCAM-1MGN-U Monochrome Global Shutter device and was calibrated using the Aruco calibration module. The lens has a nominal focal length of 3.6mm and variable length extension for Manual Focusing. For the experiments, the 45fps in 1280×960 resolution mode is used (65° Field Of View). The Ultra Wide band system used in the experiments is the PoZYX system in Precision mode.

B. Visual marker identification

The Aruco-library has various parameters that can influence the result of the identification. The minMarkerPerimeterRate variable dictates the minimum marker size to be identified, relative to the used image resolution. For the experiment, a 0.03 value is used for a 1280×0.03 = 38.4cm perimeter and $\frac{38.4}{4} = 9.6$ pixels minimum marker

width size. The Aruco markers used have a 5 bit coding plus 2bits on the sides for a total of 7 bits. The large rectangular marker size is $a = 6.9$cm on the square facets of the rhombicuboctahedron; the triangular sides include markers with size $a_s = \frac{a \sin(60^\circ)}{(1+\sin(60^\circ))} = 3.48$cm. The focal distance (f) for the proper focus on our used distances has been verified using the following formula: [Height in pixels of an object $(H(\text{px}))$ = $(f(\text{m}))$ × (real object height(m)) × (image height(px)) / $(D(\text{m}))$ × (sensor height (m))], where (f) is the focal distance of the lens and (D) the distance from the camera. In our case, $H = \frac{0.0062 \times 0.069 \times 1280}{1.3 \times 0.00846} = 49.79$ pixels. The measured object size in pixels from the grabbed image is 52 pixels, which is close to the theoretical one with the specific focal length, verifying the chosen focal distance. The maximum distance of identification for the rhombicuboctahedron is calculated as: $D = 4 \times \frac{0.5476}{38.4 \times 0.00846} = 6.7423$m. The maximum measuring distance, using the markers in the rhombicuboctahedron, in practice is around 4.6m, at which point the frequency of identified markers becomes small; a maximum distance of 2.2m is used as a reliable one to identify safely the markers and their correct orientation.

For the markers attached in the cube the maximum theoretical distance is $D = 10.65$m, whereas for experimental purposes a safe distance up to 4.7m was used for reliable identification.

C. Visual/UWB-based measurements in various angles and distances

Figure 5 presents a set of measurements that place the rhombicuboctahedron at various distances against the camera, various angles versus the camera Pitch axis $\in \{0^\circ, 10^\circ, 15^\circ, 20^\circ, 30^\circ\}$ and various yaw angles based on the solid's up vector $\in \{0^\circ, 15^\circ, 30^\circ, 45^\circ\}$. The solid forward vector (Z-axis) is always facing perpendicularly the camera $X-Y$ plane so the relative angle comparing to the camera axes is fixed. For the vertical positions 3-bins have been selected at 1, 1.5 and 2m. For the horizontal case of pitch angle 0° on the camera X axis, bins are at 0.2m, 0.5m and per 10cm from 0.9m up to 2.20m distance. The graphs in 6 and 7 present the identified distance error of the rhombicuboctahedron from the camera, versus the real distance from the camera and the Yaw angle of the solid, for the Aruco and UWB based measurements respectively.

Figure 8 presents the Yaw error of rhombicuboctahedron axis measurements using Aruco, versus the real distance from the camera and the Yaw angle of the solid.

From the aforementioned measurements, it appears that the visual technique using the Aruco-library performs best at the closer distances. The UWB based method performs reasonably well over the entire distance-range at the expense of larger distance error and larger error variance.

D. Visual measurements using a cube-solid

Figures 9 and 10 present similar measurements to the rhombicuboctahedron in the previous section, using a cube–solid which uses the same overall facet area as the truncated rhombicuboctahedron. At distances less than 0.5m the cube

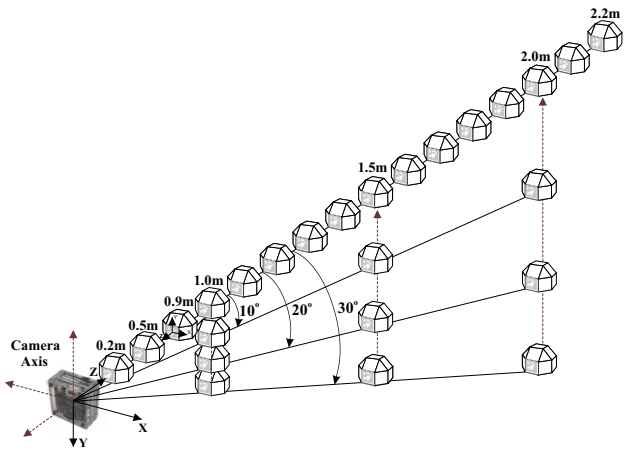

Fig. 5: Relative distance measurement locations.

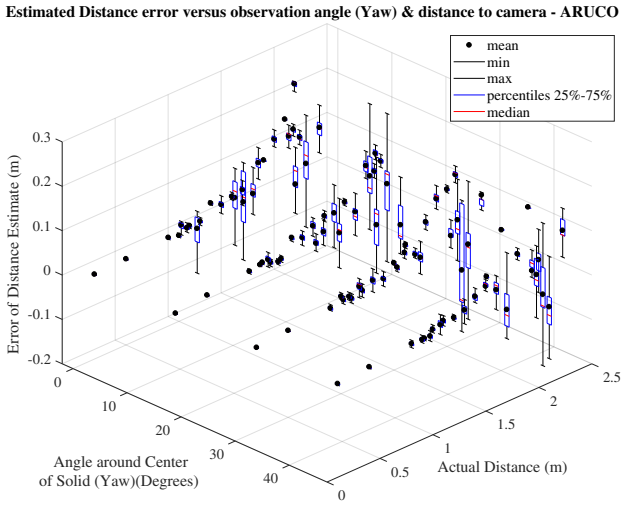

Fig. 6: Distance estimation error using rhombicuboctahedron.

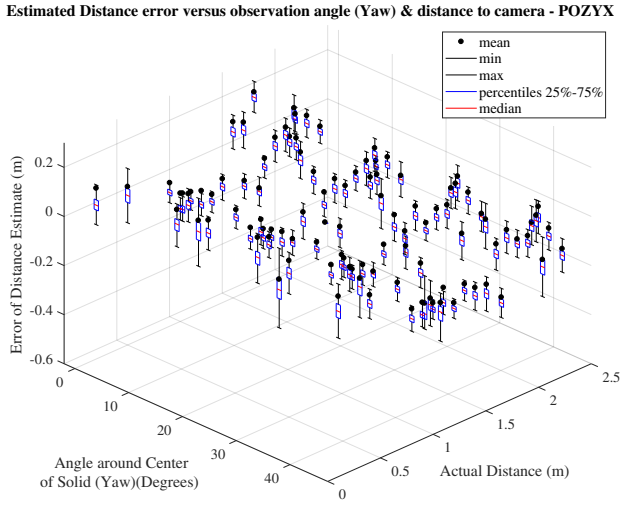

Fig. 7: Distance estimation error with UWB.

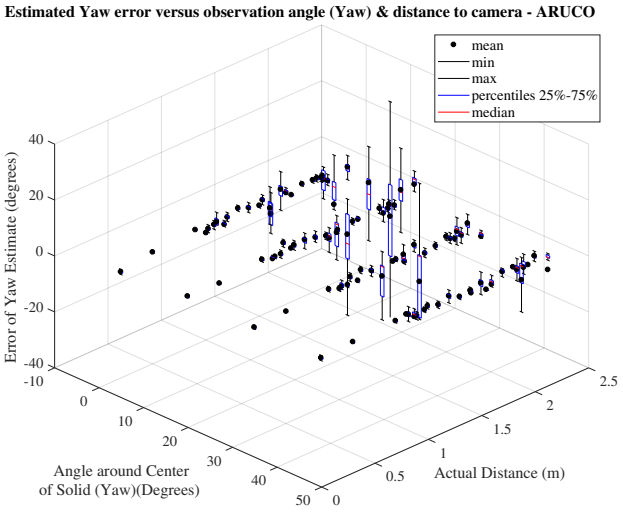

Fig. 8: Yaw estimation error using rhombicuboctahedron.

cannot provide meaningful measurements since the markers cover the entire camera's FoV because of their larger size.

In Figure 9 the identified distance error relying on the markers attached to the cube's facets using the visual method is presented, versus the real distance from the camera and the cube's yaw angle.

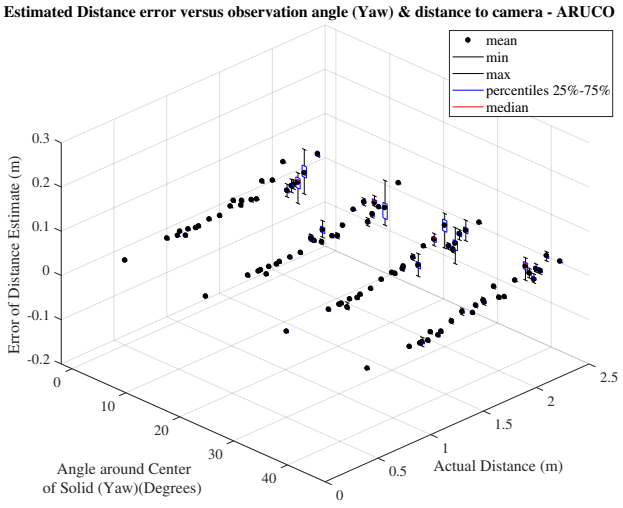

Fig. 9: Distance estimation error using a cube.

Figure 10 shows the yaw-error from the visual measurements using the cube, versus the real distance from the camera and the yaw-angle of the cube. From the previous results, we note that the cube does not provide information on the position-orientation of the drone relative to the camera at the 0.2m distance, while the rhombicuboctahedron does.

From Figures 11 and 12 we can derive that the cube has more variance in the measurements in frontal angle case, when facing the camera. These figures are similar to the ones reported in Figures 8 and 10, viewed from a different angle in the 3D graph.

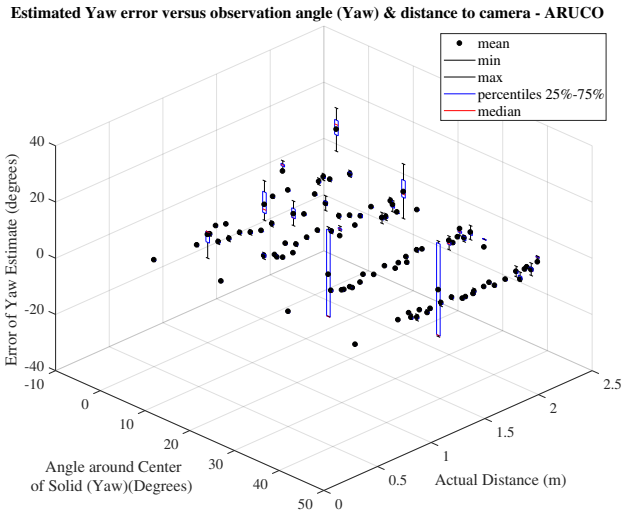

Fig. 10: Yaw estimation error using a cube.

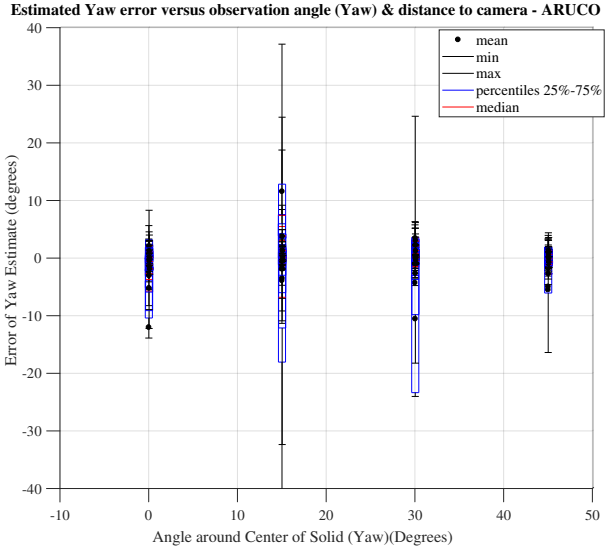

Fig. 11: Yaw estimation error with rhombicuboctahedron.

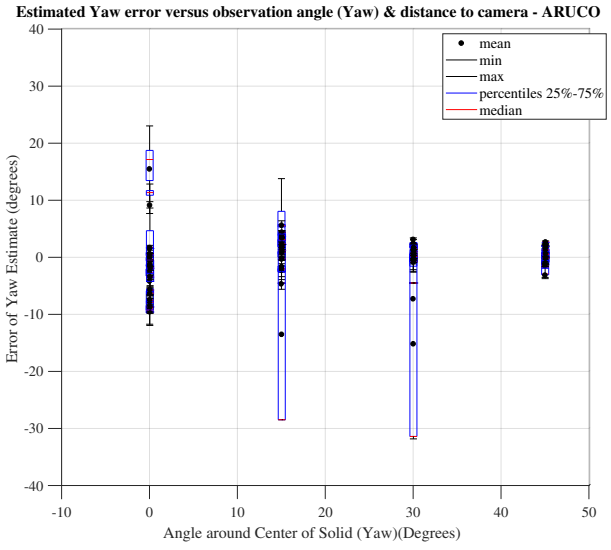

Fig. 12: Yaw estimation error with cube.

IV. UAS equipped with Fiducial Marker system

The live camera feed from the UAS (DJI Mavic Pro) camera is wirelessly transmitted at the local DJI drone controller. An Android-based custom developed software, takes the transmission as input by connecting the Android device to the controller and broadcasts it at an IP address, which is then received by the ground station as IP-camera live feed for further analysis. The UWB system is also used in fusion, in TRACKING mode to enhance the position estimation of the UAS. The two UASs communicate with each other providing their relative pose and their absolute position in relation to the base, using the UWB based system position measurements. The UWB update rate with default settings is measured at 12fps, using 1024 preamble length and in PRECISION mode. With 512 preamble length in PRECISION mode, the system provides 17fps. In FAST mode the update rate can be larger and can be setup up to 140Hz with some loss in precision of the estimated position.

The Aruco-based library executed on an i7-based computer can provide 42-44fps for the marker identification in 1280x960 resolution of the camera image. When the image is transmitted through Wi-Fi, from the UAS-Mavic Pro to Android device software and then from Android to an IP address, the measured frame rate is 10-18 fps for 720p camera feed and 3-9 fps for 1080p camera feed.

The measured latency is in the range of 530-740ms in 1080p (at 85% quality) for the overall UAS-camera feed to the ground station, 450-650ms for overall UAS to the ground station at 720p resolution and 280-290ms average latency of UAS-camera feed to the Android device. The induced large latency time indicates the need to locally process the visual feed, and not rely on the UAS's manufacturers SDKs. For this reason an Odroid XU-4 system has been employed for on-UAS experimentation; the preliminary fps have dropped to 15 fps, however the latency time is negligible.

V. Conclusions

A prototype system is developed to identify relative pose estimations among collaborating UASs. When these UASs are in close distance up to 2.2m, the visual base identification provides more accurate results. In particular the utilized rhombicuboctahedron-based system is the most accurate due to its robustness in occlusion and lighting conditions, while enjoying steady and fast identification and best orientation estimation performance. The cubic fiducial marker arrangement can be used for the middle distance case (2.2 up to 5m). The UWB based method can be used in larger distances (5m up to 30m), with a relative error of around 15cm.

References

[1] Y. Stergiopoulos, M. Thanou, and A. Tzes, "Distributed Collaborative Coverage-Control Schemes for Non-Convex Domains," *IEEE Transactions on Automatic Control*, vol. 60, no. 9, pp. 2422–2427, 2015.

[2] Y. Kantaros, M. Thanou, and A. Tzes, "Distributed coverage control for concave areas by a heterogeneous Robot-Swarm with visibility sensing constraints," *Automatica*, vol. 53, pp. 195–207, 2015.

[3] S. Papatheodorou, A. Tzes, and Y. Stergiopoulos, "Collaborative Visual Area Coverage," *Robotics and Autonomous Systems*, vol. 92, no. 9, pp. 126–138, 2017.

[4] T. Deyle, H. Nguyen, M. Reynolds, and C. C. Kemp, "RF vision: RFID receive signal strength indicator (RSSI) images for sensor fusion and mobile manipulation," in *Intelligent Robots and Systems, 2009. IROS 2009. IEEE/RSJ International Conference on*. IEEE, 2009, pp. 5553–5560.

[5] R. Liu, C. Yuen, T.-N. Do, D. Jiao, X. Liu, and U.-X. Tan, "Cooperative relative positioning of mobile users by fusing IMU inertial and UWB ranging information," in *Robotics and Automation (ICRA), 2017 IEEE International Conference on*. IEEE, 2017, pp. 5623–5629.

[6] L. Yao, Y.-W. A. Wu, L. Yao, and Z. Z. Liao, "An integrated IMU and UWB sensor based indoor positioning system," in *Indoor Positioning and Indoor Navigation (IPIN), 2017 International Conference on*. IEEE, 2017, pp. 1–8.

[7] J. Khodjaev, Y. Park, and A. Saeed Malik, "Survey of NLOS identification and error mitigation problems in UWB-based positioning algorithms for dense environments," *Annals of Telecommunications - Annales des Télécommunications*, vol. 65, no. 5, pp. 301–311, Jun 2010.

[8] M. Kok, J. D. Hol, and T. B. Schön, "Indoor Positioning Using Ultrawideband and Inertial Measurements," *IEEE Transactions on Vehicular Technology*, vol. 64, no. 4, pp. 1293–1303, April 2015.

[9] P. Müller, H. Wymeersch, and R. Piché, "UWB Positioning with Generalized Gaussian Mixture Filters," *IEEE Transactions on Mobile Computing*, vol. 13, no. 10, pp. 2406–2414, Oct 2014.

[10] E. García, P. Poudereux, A. Hernández, J. Urena, and D. Gualda, "A robust UWB indoor positioning system for highly complex environments," in *2015 IEEE International Conference on Industrial Technology (ICIT)*, March 2015, pp. 3386–3391.

[11] L. Teixeira, I. Alzugaray, and M. Chli, "Autonomous Aerial Inspection using Visual-Inertial Robust Localization and Mapping," in *Proceedings of the International Conference on Field and Service Robotics (FSR)*, 2017.

[12] E. H. C. Harik, F. Guérin, F. Guinand, J. F. Brethé, H. Pelvillain, and A. Zentout, "Vision based target tracking using an unmanned aerial vehicle," in *2015 IEEE International Workshop on Advanced Robotics and its Social Impacts (ARSO)*, June 2015, pp. 1–6.

[13] A. Benini, M. J. Rutherford, and K. P. Valavanis, "Real-time, GPU-based pose estimation of a UAV for autonomous takeoff and landing," in *2016 IEEE International Conference on Robotics and Automation (ICRA)*, May 2016, pp. 3463–3470.

[14] C. Patruno, M. Nitti, E. Stella, and T. D'Orazio, "Helipad detection for accurate UAV pose estimation by means of a visual sensor," *International Journal of Advanced Robotic Systems*, vol. 14, no. 5, pp. 1–15, 2017.

[15] W. Zheng, B. Yan, and Z. Wang, "Multi-sensor fusion based pose estimation for unmanned aerial vehicles on ships," in *2016 IEEE International Conference on Information and Automation (ICIA)*, Aug 2016, pp. 648–653.

[16] C. Kanellakis and G. Nikolakopoulos, "Survey on Computer Vision for UAVs: Current Developments and Trends," *Journal of Intelligent & Robotic Systems*, vol. 87, no. 1, pp. 141–168, Jul 2017.

[17] A. R. Vetrella, G. Fasano, D. Accardo, and A. Moccia, "Differential GNSS and Vision-Based Tracking to Improve Navigation Performance in Cooperative Multi-UAV Systems," *Sensors (Basel)*, vol. 16, no. 12, Dec 2016.

[18] S. Garrido-Jurado, R. Muñoz-Salinas, F. Madrid-Cuevas, and M. Marín-Jiménez, "Automatic generation and detection of highly reliable fiducial markers under occlusion," *Pattern Recognition*, vol. 47, no. 6, pp. 2280 – 2292, 2014.

[19] S. Garrido-Jurado, R. Muñoz-Salinas, F. J. Madrid-Cuevas, and R. Medina-Carnicer, "Generation of fiducial marker dictionaries using mixed integer linear programming," *Pattern Recognition*, vol. 51, pp. 481–491, 2016.

[20] R. Hoogervorst, S. Stramigioli, H. W. Wopereis, and M. Fumagalli, "Vision-IMU based collaborative control of a blind UAV," in *Research, Education and Development of Unmanned Aerial Systems (RED-UAS), 2015 Workshop on*. IEEE, 2015, pp. 53–61.

[21] A. C. Woods and H. M. La, "Dynamic target tracking and obstacle avoidance using a drone," in *International Symposium on Visual Computing*. Springer, 2015, pp. 857–866.

[22] M. Cheong, M. Bahiki, and S. Azrad, "Development of collision avoidance system for useful UAV applications using image sensors with laser transmitter," in *IOP Conference Series: Materials Science and Engineering*, vol. 152, no. 1. IOP Publishing, 2016, p. 012026.